



Elementary Composite Binary and Grain Alignment Locked in Dust Growth

Z. W. Hu¹  and R. P. Winarski² ¹ XNano Sciences Inc., P.O. Box 14294, Huntsville, AL 35815, USA; zwu@xnano.org² Advanced Photon Source, Argonne National Laboratory, Argonne, IL 60439, USA

Received 2021 August 25; revised 2021 October 25; accepted 2021 November 10; published 2021 December 6

Abstract

Planets are known to grow out of a star-encircling disk of the gas and dust inherited from an interstellar cloud; their formation is thought to begin with coagulation of submicron dust grains into aggregates, the first foundational stage of planet formation. However, with nanoscale and submicron solids unobservable directly in the interstellar medium (ISM) and protoplanetary disks, how dust grains grow is unclear, as are the morphology and structure of interstellar grains and the whereabouts and form of “missing iron.” Here we show an elementary composite binary in 3D sub-10 nm detail—and the alignments of its two subunits and nano-inclusions and a population of elongated composite grains locked in a primitive cosmic dust particle—noninvasively uncovered with phase-contrast X-ray nanotomography. The binary comprises a pair of oblate, quasi-spheroidal grains whose alignment and shape meet the astrophysical constraints on polarizing interstellar grains. Each member of the pair contains a high-density core of octahedral nanocrystals whose twin relationship is consistent with the magnetite’s diagnostic property at low temperatures, with a mantle exhibiting nanoscale heterogeneities, rounded edges, and pitted surfaces. This elongated binary evidently formed from an axially aligned collision of the two similar composite grains whose core–mantle structure and density gradients are consistent with interstellar processes and astronomical evidence for differential depletion. Our findings suggest that the ISM is threaded with dust grains containing preferentially oriented iron-rich magnetic nanocrystals that hold answers to astronomical problems from dust evolution, grain alignment, and the structure of magnetic fields to planetesimal growth.

Unified Astronomy Thesaurus concepts: [Interstellar dust processes \(838\)](#); [Interstellar medium \(847\)](#); [Interstellar magnetic fields \(845\)](#); [Starlight polarization \(1571\)](#); [Protoplanetary disks \(1300\)](#); [Interdisciplinary astronomy \(804\)](#); [Laboratory astrophysics \(2004\)](#); [Interstellar dust extinction \(837\)](#); [Planetesimals \(1259\)](#); [Interplanetary dust \(821\)](#); [Interstellar dust \(836\)](#); [Interstellar emissions \(840\)](#)

1. Introduction

Over the past decades, astronomers have come to appreciate that dust grains in the interstellar medium (ISM) are galactic messengers and the fundamental building blocks in star and planet formation. Yet fundamental problems remain unsolved concerning dust grains in the ISM, including their origin and formation processes; their physical properties, structure, and composition; and the whereabouts and form of “missing iron.” This may be due, in part, to the difficulty of spectroscopically characterizing dust grains conclusively.

Modeling of the zodiacal dust has indicated that cosmic dust, also known as interplanetary dust, is primarily produced by comets and Kuiper Belt objects (Nesvorný et al. 2010; Poppe 2016), with cometary breakups as the main mechanism responsible for liberating dust particles from comets into the zodiacal cloud (Nesvorný et al. 2010). This means that interplanetary dust probably provides abundant samples of the interiors of comets or icy planetesimals—remnants of the unprocessed protoplanetary aggregates of small dust grains that preserve a record of fundamental dust growth processes and physical conditions in the ISM and protoplanetary disk. Isotopic analyses have shown that primitive interplanetary dust particles (IDPs), or those exhibiting properties consistent with cometary origin, contain higher abundances of stardust (grains condensed in stellar outflows) and more pristine molecular

matter than primitive meteorites (Messenger et al. 2005; Busemann et al. 2009). Given that a typical 10 μm IDP is a fragile aggregate of, say, 10^4 – 10^5 small grains and pores that are intricately connected in 3D space (Hu & Winarski 2016), a viable way to untangle growth processes is to noninvasively unlock the structures of whole aggregate particles in 3D nanoscale detail. Being able to visualize and analyze the morphological structures of intact grains and their connections and orientations with respect to their host grains and particles in 3D is the key to understanding how dust grains grow, evolve, and clump into aggregates, which will also, in turn, yield fundamental insights into the environments where they formed and evolved.

Phase-contrast X-ray nanotomography (PCXNT) is a high-resolution and high-sensitivity X-ray nano-CT imaging technique that incorporates refraction-based phase-contrast effects into otherwise absorption X-ray nanotomography, enabling the physical structures of intact IDPs to be visualized noninvasively in 3D nanoscale detail (Hu & Winarski 2016). With high surface area-to-volume ratios, nanoscale grains are well suited to PCXNT imaging, since it relies on refraction occurring at the interfaces or edges of grains that delineate their shapes and structures, and the image contrast is formed through wave interference outside the scattering object, resulting in interface or edge enhancement. Therefore, bringing phase-contrast effects or edge enhancement into play while maintaining absorption contrast (bulk contrast) would enable us to noninvasively examine low-, medium-, and high-density grains (e.g., carbonaceous components, silicates, and Fe-rich



Original content from this work may be used under the terms of the [Creative Commons Attribution 4.0 licence](#). Any further distribution of this work must maintain attribution to the author(s) and the title of the work, journal citation and DOI.

minerals) throughout an entire particle in a detailed manner that is otherwise unobtainable.

In this paper, we report the discovery of an elementary composite binary (termed an “astrobinary” for simplicity) whose intragrain alignment and properties (component shapes and sizes and microstructural and compositional heterogeneities) are consistent with the constraints on interstellar grains set by polarization and depletion (Sofia et al. 1994; Kim & Martin 1995; Martin 1995; Savage & Sembach 1996; Draine 2011; Andersson et al. 2015; Draine & Hensley 2021), as well as the hidden alignment of elongated grains locked in the host particle that is unexpected from Brownian motion-driven growth in the protoplanetary disk. The sub-10 nm detail of the astrobinary nondestructively revealed by PCXNT provides direct evidence for its interstellar origin and an up-close 3D view of grain growth and grain alignment, two of the outstanding problems in astronomy that are the subjects of ongoing research (Draine 1990, 2003, 2011; Andersson et al. 2015; Dwek 2016; Hoang & Lazarian 2016; Zhukovska et al. 2018; Draine & Hensley 2021). The discovery of the astrobinary containing the clusters of oriented nanocrystals exhibiting properties consistent with those of magnetic inclusions of magnetite (Fe_3O_4) yields fresh insights into dust growth and alignment and their connection and a likely solution to the long-standing conundrum of the form of iron incorporated into dust grains (Draine & Hensley 2013; Dwek 2016; Zhukovska et al. 2018).

2. Experimental Methods

Experimental methods and principles are described concisely in this paper, with more information on experiments including sample mounting and PCXNT imaging principles referring to our previous work (Hu & Winarski 2016). Experiments were performed using highly coherent 10 keV X-rays with a beam pass, $\Delta\lambda/\lambda$, of $\sim 10^{-4}$ on the Center for Nanoscale Materials (CNM)/X-ray Science Division Hard X-ray Nanoprobe Beamline (26-ID) at the Advanced Photon Source (APS), Argonne National Laboratory (Winarski et al. 2012). The IDP U2015-M-1 was mounted on the top of a tungsten needle tip and imaged under a full-field transmission mode. A reflective ellipsoidal capillary with high focusing efficiency ($\sim 90\%$) and a high numerical aperture matching the objective lens was employed to provide a focused undulator beam to fully illuminate the particle mounted on the rotation stage to allow transmission images to be acquired between $\pm 90^\circ$ at an angular interval of 0.1° . A high-resolution Fresnel zone plate with an outermost zone width of 24 nm was used as the objective lens to magnify the projection images, which, combined with a lens-coupled CCD imaging system with a dynamic range of 0–65,535 positioned downstream from the sample for phase-contrast imaging, resulted in an effective pixel size of $15.75 \times 15.75 \text{ nm}^2$ on the recorded transmission images. A Zernike phase ring was placed in the back focal plane of the objective lens to maximize phase-contrast effects. Positional shifts due to rotational wobble and gravitational drift were corrected to ensure high-quality reconstructed images. High-contrast and high-sensitivity X-ray nanotomography imaging enables us to resolve subvoxel-sized features, including high-density nanoparticles. We used classical volume rendering with Amira to analyze grains and nano-inclusions in 3D. Maximum intensity projection was combined to reveal the highest-intensity (highest-attenuation) voxels in the volume of data

along the lines of sight (in maximum intensity projection, the shapes and relationships of inclusions and grains may be obscured due to its 2D nature, especially when they overlap).

3. Results and Discussions

The $\sim 10 \mu\text{m}$ primitive IDP we examined is shaped like a quasi-ellipsoid that is somewhat flattened along the short axis, with a long-to-short axis ratio of about 2.2 (Figure 1(a)). The particle, with its pore structure consisting of primitive submicron-sized intergranular voids and intragranular nano-holes and bearing no trace of parent-body processing (Hu & Winarski 2016), is a fine-grained aggregate containing two morphologically distinct types of refractory grains: irregular, elongated grains that represent a major grain population and often constitute highly porous subaggregates and hollow grains that each have a nanohole running through the core (Figure 1(b)) and are morphologically consistent with refractory carbonaceous or organic globules that were demonstrated in our previous study (Hu & Winarski 2016). The elongated grains have long-to-short axial ratios ranging from about 2.2 to 3.3, in agreement with a mean aspect ratio (~ 2.87) of the elongated comet 67P grains acquired through an atomic force microscope on board Rosetta (Bentley et al. 2016). In addition, the elongated grains tend to be mutually aligned, with a preferred orientation along the particle’s long axis (e.g., grains A–F, Figures 1(b) and (c)). Hollow grains, on the other hand, appear to be randomly oriented with respect to each other (Figure 2). This “selective grain alignment” could not result from secondary processing. For example, strong atmospheric entry heating would have destroyed or masked the ordered grain arrangement due to thermal alteration (Hu & Winarski 2016). It is also hard to conceive of a parent-body process that could make one particular group of dust grains reorient without breaking the host particle’s cohesive structure, not to mention the evidence to the contrary (Hu & Winarski 2016). The observation that the elongated grains are aligned, with their long axes tending to be along the host particle’s long axis, respectively, shows that the grain alignment was locked in place during dust growth.

The aligned elongated grains have complex morphologies in 3D. Grain E (Figures 1(b) and (c)), with an axial ratio of about 3.3, turns out to be a binary grain or the astrobinary, consisting of two almost equal-sized, oblate, quasi-spheroidal subunits or grains connected by a narrower part, or neck (arrow in Figure 3(a)). The lower and upper grains of this astrobinary have long, intermediate, and short semiaxes of about $103 \times 87 \times 55$ and $103 \times 87 \times 63$ nm, respectively, and the neck is estimated to be ~ 15 nm long and ~ 55 nm in radius. The pair are almost perfectly aligned axially, resulting in an elongated binary whose overall shape resembles Arrokoth’s (Stern et al. 2019), although the former is approximately 10^{11} times smaller than the latter in size. The morphology of this astrobinary nondestructively uncovered in 3D is consistent with collisional grain growth or grain coagulation, a physical process in which two colliding grains with a low relative velocity stick together to form a larger grain (Draine 1990; Chokshi et al. 1993; Dominik & Tielens 1997; Blum & Wurm 2008). A contact neck is formed by the deformation caused by pushing and pulling during the collision process or by the combined deformation and migration of water molecules (for icy grains) according to theoretical modeling (Chokshi et al. 1993; Dominik & Tielens 1997; Blum & Wurm 2008;

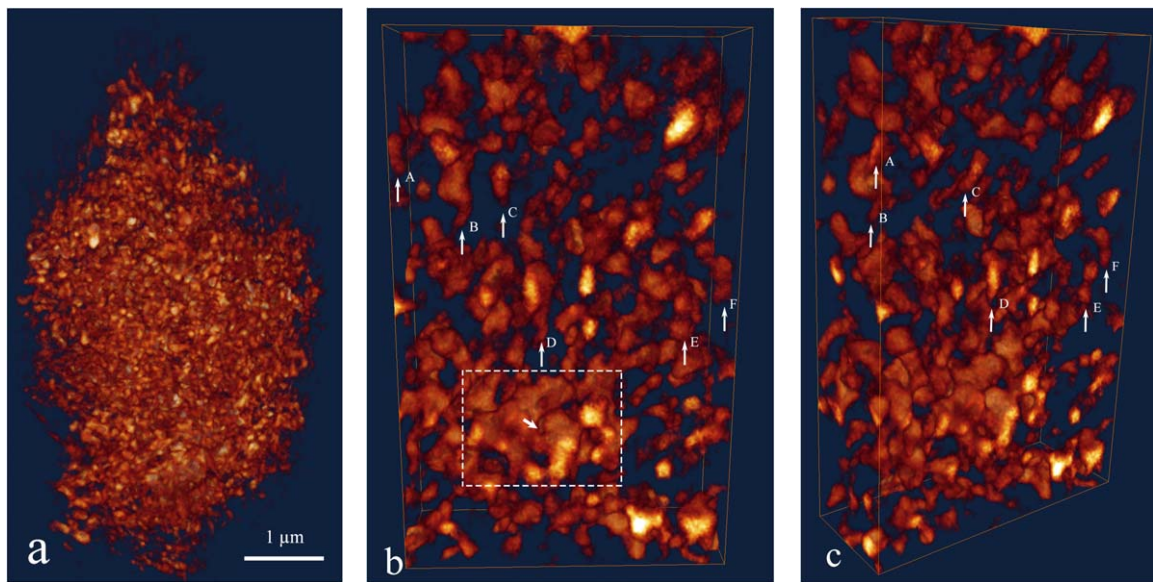


Figure 1. Quasi-ellipsoidal IDP U2015-M-1 containing preferentially oriented elongated grains (e.g., grains A–F in panels (b) and (c)). (a) Volume-rendered image of the entire particle from PCXNT data. (b) and (c) Volume-rendered images of internal structure viewed from two different angles. A cluster (dashed rectangle in panel (b)) contains hollow grains, with one indicated by an arrow (see Figure 2(c)). Volume: $0.9 \times 2.3 \times 3.7 \mu\text{m}^3$.

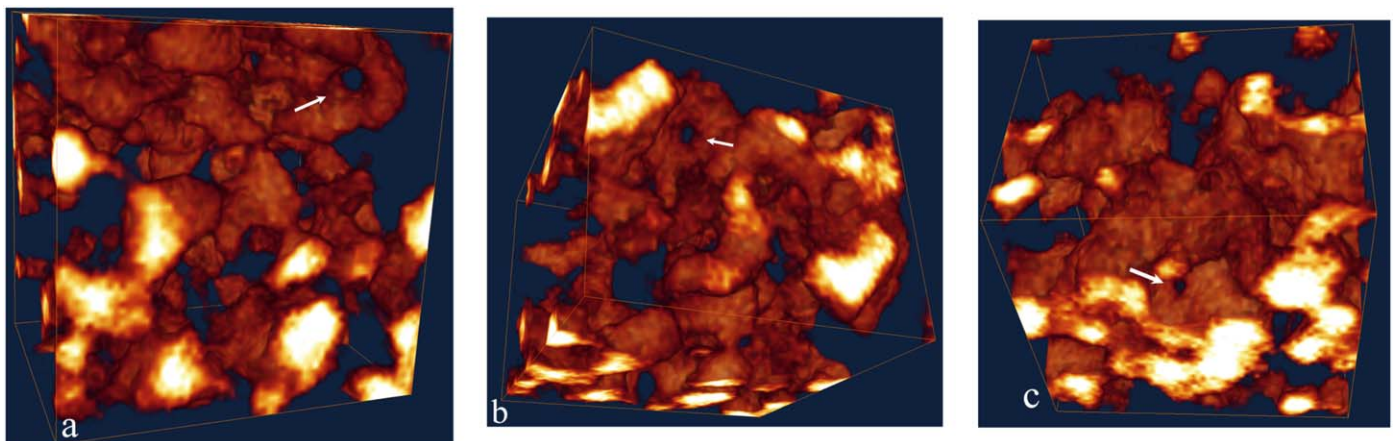


Figure 2. Hollow grains exhibit no obvious preferred orientation with respect to the host IDP. (a) and (b) Volume-rendered image of hollow grains (arrows) viewed from two different angles. The nanohole of the grain (arrow in panel (a)) is hidden in panel (b), with its orientation considerably different from that of the grain (arrow in panel (b)), although the two are in the same cluster. (c) Volume-rendered image showing the hollow grain (arrow in Figure 1(b)) with the nanohole revealed by tilting forward and sideways relative to Figure 1(b). Volume: $0.8 \times 1.0 \times 1.0 \mu\text{m}^3$.

Sirono & Ueno 2017). This astrobinary is located in the interior of such a primitive IDP that experienced no appreciable parent-body alteration and escaped significant atmospheric entry heating, as evidenced by well-preserved, morphologically primitive intergranular voids and pristine hollow grains (Hu & Winarski 2016). The revelation that the astrobinary is made up of the two grains of similar size and shape shows that this is a “morphologically pristine” elementary binary. The term “morphologically pristine” means that the geometry of the original pair per se has been preserved, although surface alterations may or may not have occurred since its formation.

Unlike the euhedral crystals of olivine and pyroxene forming equilibrated aggregates of ~ 0.1 – $1 \mu\text{m}$ in diameter observed in some IDPs (Bradley 1994), this morphologically distinct binary is composed of two composite grains, each with a heterogeneous mantle and a cluster of preferentially oriented, twinned octahedral nanocrystals of \sim sub-10 to several tens of

nanometers in size as the inner grain core (Figures 3 and 4). The nanocrystal inclusions exhibit rather flat, faceted surfaces, in contrast to the irregularly shaped mantle with overall rounded edges and cratered or pitted surface layers (a source of porosity). This striking difference between the nanoinclusions and mantle provides strong evidence that the nanocrystals were shielded from destruction by interstellar shocks while the exteriors of the growing grains were altered by interstellar processes along the way, including erosion by sputtering, cratering, shattering and/or vaporization by grain–grain collisions, and accretion (Jones 2001; Draine 2003). The nanocrystals appear brightest in bulk contrast (Figure 3), meaning they have very high densities. They are morphologically and texturally different from Fe-rich sulfide and the Fe–Ni phases observed in IDPs and in and on GEMS (Bradley 1994; Ishii et al. 2008; Keller & Messenger 2011). Their octahedral habit (external shape) instead is consistent with the characteristic habit of naturally occurring

single crystals of cubic magnetite that are octahedra bounded by the eight $\{111\}$ planes (The Miller indices 111 in curly brackets, $\{111\}$, denote a set of 8 symmetry-equivalent planes or faces in the cubic crystal, including (111) plane and 7 other planes with the negative of any of those Miller indices or integers. The (111) denotes a specific crystal plane (as opposed to a set of planes by $\{111\}$), which intersects the crystallographic axes at (1,0,0), (0,1,0), and (0,0,1)). (Magnetite is a ferrimagnetic mineral that is spontaneously magnetized along its easy axis and strongly magnetic even at room temperature. Its ferrimagnetism is attributed to its cubic inverse spinel structure, where the two magnetic sublattices formed from the tetragonal (A) and octahedral (B) cation sites, respectively, have antiparallel spins below the Curie temperature, but their magnetic moments are unequal in magnitude, resulting in a net magnetic moment (Cornell & Schwertmann 2003)). Moreover, the octahedral nanocrystals are twinned with orthogonal long axes (Figures 3(b), (c), and (e)), consistent with the monoclinic twins with orthogonal c -axes (easy axes) developed during the magnetite’s cubic-to-monoclinic phase transition at the Verwey transition temperature T_v of ~ 120 K (Özdemir & Dunlop 1999; Lindquist et al. 2019). (The Verwey transition is unique to magnetite and can be used to distinguish magnetite from maghemite and greigite; Cornell & Schwertmann 2003). During the first-order phase transition, magnetite’s crystal structure changes from high-symmetry cubic (Fd-3m) above T_v to low-symmetry monoclinic (Cc) below T_v by a slight lattice distortion, accompanied by the development of ferroelastic or crystallographic twins in the monoclinic phase that has strong magnetocrystalline anisotropy. Its magnetic easy axis switches from the cubic $\langle 111 \rangle$ directions to the monoclinic $[001]$, and any of the three cubic $\langle 001 \rangle$ axes may become the easy axis or c -axis in the monoclinic phase (Özdemir & Dunlop 1999; Lindquist et al. 2019). (Miller indices in square brackets such as $[001]$ and angle brackets such as $\langle 001 \rangle$ denote a specific direction and a set of symmetry-equivalent directions, respectively. The cubic directions represent eight symmetry-equivalent directions, including $[111]$ and seven others with the negative of any of those Miller indices or directions, and they are the normal to the $\{111\}$ planes in the cubic crystal system.) The nanocrystal inclusions (Figure 3), if they are magnetite (as indicated by their distinct shape), must have undergone the Verwey transition at some point in their growth or evolution and remained monoclinic during subsequent growth, given that interstellar grain temperatures are below T_v (Draine & Hensley 2013). This is what happened, as evidenced by the development of the twinned nanocrystals (Figure 3). Each of the nanocrystals per se must be a single magnetic domain (behaving like a single strong magnetic dipole), given that their sizes are smaller than the critical size of single-domain magnetite nanoparticles (Li et al. 2017). The single-domain nanocrystals forming a twin structure is a manifestation of the occurrence of the Verwey transition in the cold ISM, and the twin domains with the orthogonal c -axes (the long axes running through the opposite vertices of the elongated octahedra) correspond to type 1 twins observed in large multidomain octahedral crystals of natural magnetite (Lindquist et al. 2019). With the Verwey transition inducing a spontaneous strain due to the lowering of symmetry, twinning of the single-domain magnetite crystals with orthogonal c -axes is energetically favorable. The clustered nanoinclusions may well have stayed below the blocking temperature (above which nanocrystals become superparamagnetic) during grain growth in

a dense molecular cloud. The twin structure is well preserved, where the nanocrystals are twinned with the orthogonal easy axes that tend to be either parallel or perpendicular to the astrobinary’s long axis (Figures 3(b) and (e)). Iron oxides present in interstellar grains were first hypothesized to explain grain alignment with superparamagnetic relaxation (Jones & Spitzer 1967). The revealed nanocrystals, unlike the secondary polycrystalline magnetite rims formed on strongly heated IDPs (Bradley 1994), are well-faceted and preferentially oriented, indicating their pristine state. The pair’s near-perfect alignment and shape suggest that the grain mantle is not primarily carbonaceous material but rather a “dirty silicate” (one with less densely embedded high-density nanoparticles that appear to be oriented like those in the grain core). Carbonaceous grains are not appreciably aligned according to spectropolarimetric observations (Chiar et al. 2006). The pair’s density appears to vary on the nanoscale, decreasing from core to surface (Figures 3 and 5), which implies a falling ratio of Fe to Mg from core to surface (the effect of thickness variation is negligible, as the slice of the pair (Figure 4) is found to exhibit an attenuation variation pattern like that in Figure 5). The revealed core–mantle structure and density heterogeneities at the nanoscale, as well as the morphological and textural differences between the nanoinclusions and grains, suggest that the relatively larger nanocrystals with the highest density formed first and that they acted as substrates or nuclei for sequential grain growth by accretion of atoms and matter in the cold ISM. The density heterogeneities or gradients from core to surface were a direct result of the interstellar processes. The high-density nanocrystal inclusions most likely played a crucial role in subsequently aligning the pair and shaping the astrobinary that has a core/mantle grain structure generally consistent with the astronomical evidence for differential depletion and resilient Fe-rich oxide cores and silicate mantles, as drawn from interstellar elemental depletion patterns obtained with the Hubble Space Telescope (Sofia et al. 1994; Martin 1995; Savage & Sembach 1996).

The grains in the pair are aligned with their short axes (the axis of greatest moment of inertia among the three principal axes) highly parallel to each other, which is consistent with the interstellar grain alignment inferred from starlight polarization and predictions by the theory of radiative torque (RAT) alignment in the ISM (Draine 2011; Andersson et al. 2015; that is, larger interstellar grains (say, >50 nm) are aligned with their short axes tending to be parallel to the magnetic field by RATs when exposed to anisotropic radiation. It has been shown that magnetic or superparamagnetic relaxation alone cannot align grains efficiently due to inefficient internal relaxation (Roberge & Lazarian 1999; Hoang & Lazarian 2016). Interstellar grains with magnetic inclusions, however, can be perfectly aligned through magnetically enhanced RAT alignment according to numerical modeling, which has been proposed as a way (if required) to interpret Planck data that show a high degree of dust polarization (Hoang & Lazarian 2016). Random gas–grain collisions in the ISM tend to disorient grains, not to mention that aligning them along their short axis is hardest among the three principal axes, which would require the greatest torques applied on the pair systematically. The way the pair is oriented suggests that it became aligned with respect to the magnetic field prior to and/or during collision. In this scenario, the two spinning grains would make contact with each other along their long axes and readily stick together thanks to low relative translational motion induced by gas collisions, leading to a

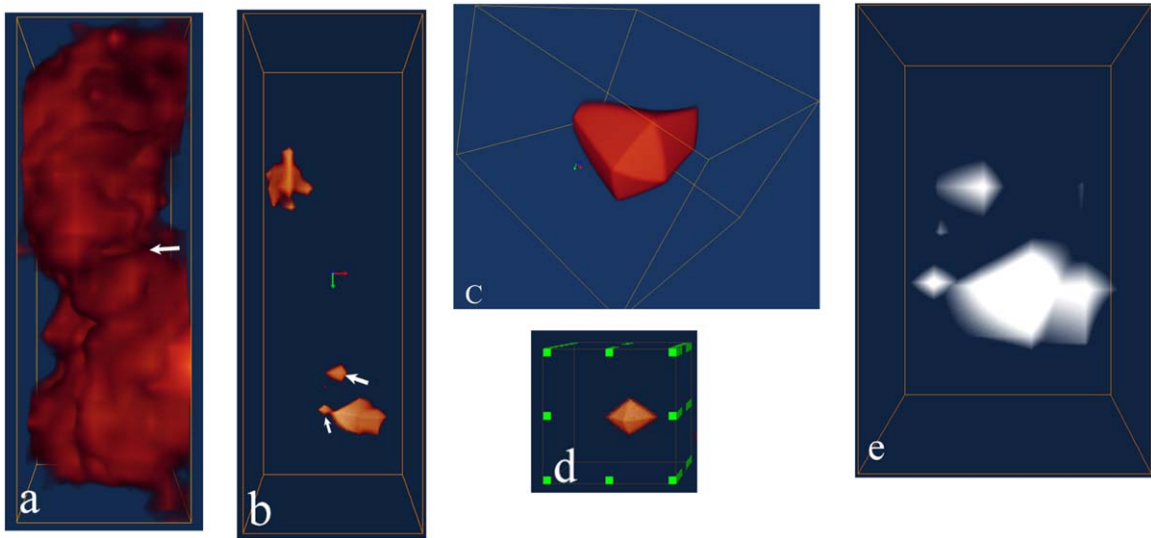


Figure 3. The astrobinary consists of two axially aligned grains containing clusters of twinned octahedral nanocrystals of high density. (a) and (b) Volume-rendered images showing the astrobinary and twinned nanocrystals, respectively. Red, green, and blue arrows in panel (b) denote the X -, Y -, and Z -axes. (c) Close-up of twinned octahedra (larger arrow in panel (b)) with orthogonal elongated axes (~ 20 nm long). (d) Close-up of a small octahedral nanocrystal (small arrow in panel (b)) before its twinning with a crystal to the right. The green cube is the voxel size 15.75^3 nm 3 . (e) Maximum intensity projection close-up of the nanocrystal cluster in the lower grain. Bright linear features running across the nanocrystals are primarily phase contrast that appears at their edges, overlapping bulk absorption contrast. A protrusion at the top right is a portion of its neighbors. The volume is $157.50 \times 173.25 \times 425.25$ nm 3 for panels (a) and (b), $47.25 \times 63 \times 63$ nm 3 for panel (c), and $94.50 \times 141.75 \times 141.75$ nm 3 for panel (e).

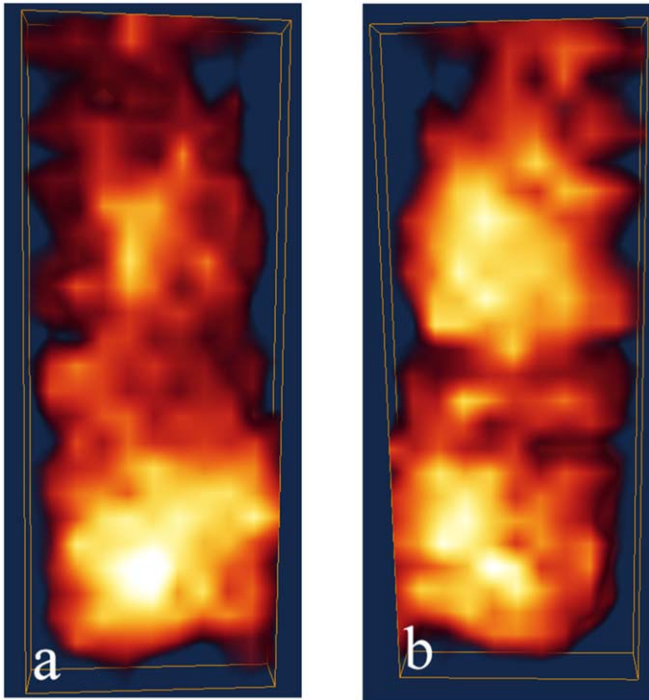


Figure 4. The astrobinary’s two subunits bear similar traces of partial destruction, except the faceted nanocrystals in the cores that are uniformly solid and smooth (Figure 3). (a) and (b) Volume-rendered images of the binary’s interior slicing through the grain cores (brighter), viewed at angles of about $\pm 90^\circ$ to Figure 3(a), respectively. Apparent zigzag-like outlines are due to uneven surfaces. Bright linear features that appear vertically and horizontally result from phase-contrast effects occurring at the edges of oriented nanoinclusions, as seen from Figure 3(e). The brightest spots correspond to portions of the larger nanocrystals. Volume: $47.25 \times 173.25 \times 425.25$ nm 3 .

contact binary with their alignment locked in place. It is noted that the geometric cross section along the grain’s short axis (the alignment axis) is larger than that in the grain’s long axis.

Grains’ magnetic anisotropy caused by the twinned magnetic inclusions with orthogonal easy axes may have played a role in enhancing the effective cross section along the grain’s long axis when they approached each other to form a nanodumbbell-like binary instead of a sandwich-like binary. Exactly how the binary structure is formed needs to be further studied, together with relevant laboratory experiments on dust grains (a new paper (Hoang 2021), which studies the effect of internal and external grain alignment on dust growth under different conditions, shows that dust coagulation can lead to the formation of elongated binaries with their components aligned along their short axes). Reasonably approximating the pair as two oblate spheroids gives a long–short axial ratio of about 1.7 and 1.5 for the lower and upper grains (Figure 3(a)), respectively, which, along with their estimated porosity ($\sim \leq 25\%$), is comparable to the axial ratios and low porosities of interstellar grains as constrained by the observed starlight polarization and polarized submillimeter emissions (Kim & Martin 1995; Draine & Hensley 2021). Our results demonstrate that this refractory astrobinary meets the astronomical constraints and is a “morphologically primordial” elementary binary—one formed in the ISM—and its geometry or structural integrity survived intact from the initial phases of solar system formation. This is consistent with the view that most of the interstellar dust falling into the outer regions of accretion disks from molecular cloud cores remains unaltered during its transit through the weak shock front (Beckwith et al. 2000; Ehrenfreund et al. 2004). The astrobinary grain and other elongated grains became aligned (Figures 1(b) and (c)) by the interactions of grains with one another, the medium, or both during subsequent growth in the protoplanetary disk.

However, the observed grain alignment would not have been expected to occur based on the common assumption that submicron or smaller grains are well coupled to the gas in protoplanetary disks and that grain coagulation is governed by Brownian motion (contributions to collisional growth due to

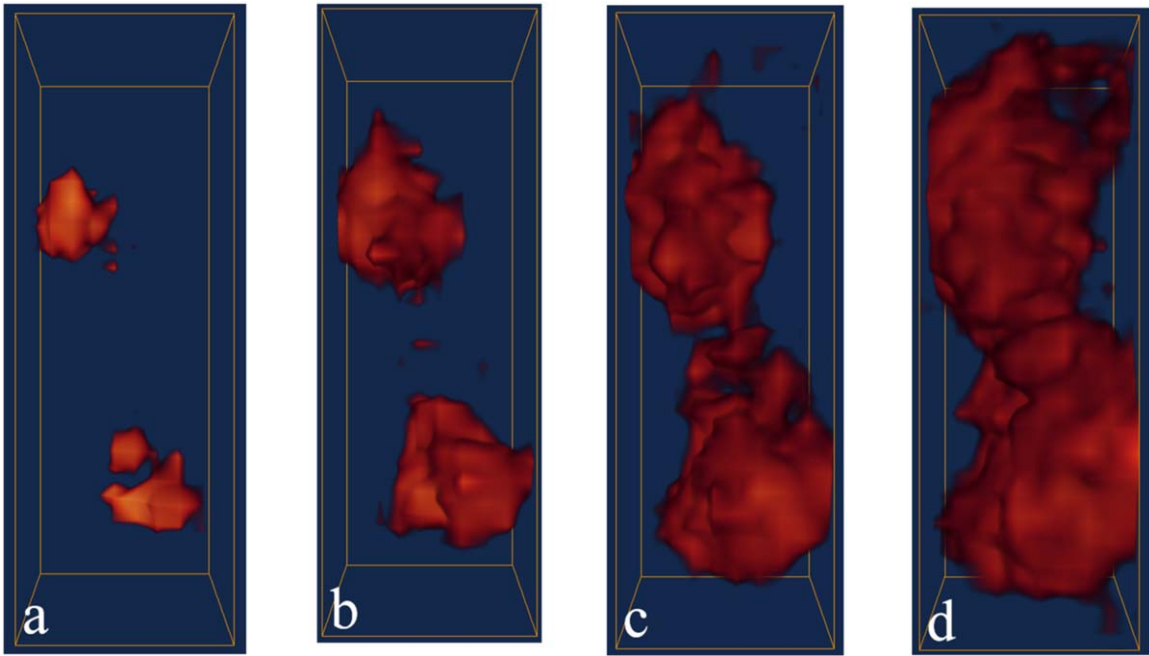


Figure 5. A set of volume-rendered images of the astrobinary shows that the pair exhibits a similar attenuation variation pattern indicative of the highest density of material at the core and the lowest density of material at the outermost layer. The images were produced by sequentially varying the display transparency within the range defined by high (Figure 3(b)) and low (Figure 3(a)) thresholds. Volume: $157.50 \times 173.25 \times 425.25 \text{ nm}^3$.

turbulence and settling are believed to be negligible for such small grains; Blum & Wurm 2008; Birnstiel et al. 2016). Agglomerated grains in this growth scenario should be randomly oriented with respect to one another, since sticking grains together by mutual attraction (e.g., van der Waals forces) is realized through random gas–grain collisions. That assumption has also been challenged by the latest results on the heights of gas and dust grains in protoplanetary disks obtained with the Atacama Large Millimeter/submillimeter Array and near-IR polarized light (Rich et al. 2021). (Coagulation of submicron grains into micron-sized aggregates may also occur in molecular clouds. However, complex grain alignment behavior and diverse dust grains present in the IDP suggest that this dust particle was originally formed in the outer protoplanetary disk.) The astrobinary, grain E (Figure 1), is the most pristine binary identified yet. Grains A, B, C, D, and F (Figures 1(b) and (c)) may be binary. On average, the elongated grains A–F are oriented with respect to the quasi-spheroidal IDP, with their short and long axes aligned $\sim 21^\circ$ and $\sim 12^\circ$ from the IDP’s short and long axes, respectively. The grains containing at least a cluster of densely packed high-density nanocrystals (grains B, D, E, and F) appear to be better aligned lengthwise (with their long axes parallel to the particle’s long axis) than those with only less densely embedded nanoparticles (grains A and C). The hollow grains uncovered to date are all present in compact clusters with complex shapes, which makes it hard to see their real shapes and define their principal axes reliably. They probably belong to a population of carbonaceous dust grains or are largely made of carbonaceous material. How they are oriented or aligned with respect to the astrobinary and the host particle needs to be further investigated. Regardless of the detailed physics of alignment mechanisms, the grain alignment revealed in the IDP implies that the forces and aligning torques applied to the elongated grains with high-density nanoparticles were strong enough to overcome the randomizing effects of gas collisions to effect dust growth.

4. Summary and Implications

We have discovered an elementary composite binary whose intragrain alignment and grain shape and size are generally consistent with the astronomical constraints on polarizing interstellar grains. The morphological and microstructural details of the intact binary revealed in 3D show that this astrobinary consists of a pair of axially aligned, nearly equal-sized composite grains containing clusters of preferentially oriented octahedral nanocrystals of high density that are twinned with their orthogonal long axes tending to be either parallel or perpendicular to the binary’s long axis and their properties consistent with magnetite’s diagnostic properties. Each member of the pair exhibits nanoscale density heterogeneities from core to surface, as well as rounded edges and cratered surfaces, consistent with interstellar elemental depletions and interstellar processing. This astrobinary, a “survivor” of the initial stages of solar system formation, was uncovered noninvasively from a primitive, quasi-ellipsoidal cosmic dust particle in which the astrobinary and other elongated composite grains are also aligned but in a more complicated way, indicative of the two different environments where the astrobinary and host particle were formed.

The existence of the composite astrobinary with the preferentially oriented nano-inclusions exhibiting properties consistent with magnetic magnetite is likely to have broad and important astronomical implications. The issue concerning the formation and evolution of dust grains in the ISM, initially arising from attempting to develop a theory of interstellar polarization about 70 yr ago (Spitzer & Tukey 1951), has become fundamentally important for understanding star and planet formation. While the high depletions of refractory elements observed in the gas phase support the view that most interstellar dust was formed in the ISM, questions have remained unsettled concerning how dust grains form and evolve in the ISM (Draine 2003; Dwek 2016; Zhukovska et al. 2018). The distinct binary with the core–mantle grain structure noninvasively uncovered in 3D sub-10 nm detail

provides direct evidence of grain growth and alignment and their connection, as well as interstellar processing, yielding fresh insights into the formation and evolution of interstellar dust grains. The findings suggest that at least a population of polarizing interstellar grains are complex composite grains that contain clusters of preferentially oriented high-density nanocrystals encased in “dirty amorphous silicates” (those with less densely embedded high-density nanoparticles), being overall elongated and/or flattened to varying degrees (depending on whether they are single- or multicomponent structures). Iron is extremely depleted in the gas phase relative to solar abundances, and 90% or more of the total iron is thought to be incorporated into dust grains somehow, a key element for understanding the origin and evolution of interstellar dust (Dwek 2016; Zhukovska et al. 2018). Our observations yield a probable solution to the long outstanding problem of the whereabouts and form of the “missing iron” (Draine & Hensley 2013; Dwek 2016; Zhukovska et al. 2018). The well-preserved clusters of twinned octahedral nanoinclusions in the astrobinary, as well as the nanoscale density heterogeneities from core to surface, imply that iron-rich magnetic nanocrystals functioned as nuclei or substrates for sequential grain growth and regrowth. The presence of preferentially oriented magnetic nanoinclusions in interstellar grains will have consequential effects on grain alignment properties and polarized emission at microwave and submillimeter frequencies (Draine & Hensley 2013). Characterizing and understanding the physical properties of magnetic nanocrystals and clusters will be critical to understanding interstellar grain growth and alignment but also to the success of cosmic microwave background polarization experiments in search of primordial gravitational waves (Planck Collaboration XI 2020). Being able to visualize and analyze grains and nanoinclusions and grain alignment in situ in intact host particles in 3D sub-10 nm detail is opening up a new opportunity to probe their origin and formation mechanisms in detail and gain in-depth insights into grain alignment properties and the structure of the magnetic fields in the ISM and protoplanetary disks. The findings also raise new questions on the detailed physics of interstellar dust growth and grain alignment, which will need to be addressed through systematic sample analysis, in conjunction with laboratory experiments (including those in microgravity) and theoretical modeling among the members of the broad astronomical community. As demonstrated above, the sticking together of two axially aligned, oblate, quasi-spheroidal grains leads to an elongated, prolate, quasi-spheroidal binary with a relatively flattened shape and a low porosity of $\sim \leq 25\%$ ($\sim \leq 40\%$ if a fluffy, ultrathin mantle is taken into account, which appears discernible but needs to be further studied). Likewise, sticking aligned elongated grains together results in a larger, elongated aggregate (in the present case, the elongated, quasi-ellipsoidal IDP is an aggregate of aligned elongated grains and apparently nonaligned grains or clusters). This is of potentially fundamental importance to planetesimal and planet formation, as Brownian motion-driven coagulation is too slow to explain apparently robust planetesimal growth (Kempf et al. 1999). Long-range attractive forces between the opposite poles of magnetic grains increase collision cross sections by, say, orders of magnitude compared with Brownian motion-driven growth (Nuth & Wilkinson 1995; Dominik & Nübold 2002), as well as the relative velocity and number density of grains, which will, in turn, increase collision frequency and dust growth rates (Birnstiel et al. 2016). More important, grains with magnetic


inclusions or large magnetic dipoles will readily line up with or by the ambient magnetic field on a large scale and cluster together more efficiently, resulting in rapid growth of larger aggregates. Hence, the magnetically enhanced dust growth process may be robust and rapid enough to overcome growth barriers (Blum & Wurm 2008; Testi et al. 2014; Birnstiel et al. 2016; Cuzzi et al. 2017) and produce centimeter-sized or larger aggregates within dense layers of the disk, leading to planetesimals via the streaming (Nesvorný et al. 2019) or clustering instability (Cuzzi et al. 2017), or by running its course, especially when sticky ices get involved. In other words, some of the first planetesimals in our solar system may have grown out of the outer protoplanetary disk. As IDPs collected in the stratosphere experience atmospheric entry heating, which is a major limiting factor in maximizing the scientific value of cosmic dust, it is of paramount importance to collect pristine cometary dust particles for laboratory studies to test hypotheses and address fundamental questions concerning dust evolution, planet formation, and the origin of life in detail.

The presence of the elementary composite binary with its properties overall consistent with the astronomical constraints on polarizing interstellar grains also underscores the importance of in situ measuring interstellar dust grains across the heliopause (the boundary between the heliosphere and the local ISM) in order to gain a true picture of the properties of interstellar dust grains and the interaction between interstellar dust and the heliosphere, including how interstellar grains are filtered by the heliosphere (Slavin et al. 2012). (Results obtained from in situ measurements of interstellar dust thus far do not appear to agree with astronomical observations.) Our observations suggest that binaries and oblate, quasi-spheroidal elongated grains containing iron-rich magnetic nanocrystals are highly aligned with the interstellar magnetic field. In situ measurements of the properties and trajectories of dust grains across the local ISM and the heliopause, combined with dust polarization measurements, may allow the structure of local magnetic fields across the regions to be mapped in detail to constrain the 3D shape of the heliosphere (Reisenfeld et al. 2021).

Z.W.H. thanks J. N. Cuzzi, J. Blum, and many other researchers for lively discussions at Accretion: Building New Worlds Conference, and the NASA/JSC cosmic dust curatorial staff for providing cosmic dust particles for this research. Use of the CNM and APS was supported by the DOE, Office of Science, Office of Basic Energy Sciences, under contract No. DE-AC02-06CH11357. The work was partly funded by NASA grant NNX12AP38G. We thank an anonymous reviewer whose insightful comments resulted in improvement in the manuscript.

ORCID iDs

Z. W. Hu  <https://orcid.org/0000-0002-7864-8830>

R. P. Winarski  <https://orcid.org/0000-0002-6885-5983>

References

- Andersson, B.-G., Lazarian, A., & Vaillancourt, J. E. 2015, *ARA&A*, **53**, 501
- Beckwith, S. V. W., Henning, T., & Nakagawa, Y. 2000, in *Protostars and Planets IV*, ed. V. Mannings, A. P. Boss, & S. S. Russell (Tucson, AZ: Univ. of Arizona Press), 553
- Bentley, M. S., Schmied, R., Mannel, T., et al. 2016, *Natur*, **537**, 73
- Birnstiel, T., Fang, M., & Johansen, A. 2016, *SSRv*, **205**, 41
- Blum, J., & Wurm, G. 2008, *ARA&A*, **46**, 21

- Bradley, J. P. 1994, *GeCoA*, **58**, 2123
- Busemann, H., Nguyen, A. N., Cody, G. D., et al. 2009, *E&PSL*, **288**, 44
- Chiar, J. E., Adamson, A. J., Whittet, D. C. B., et al. 2006, *ApJ*, **651**, 268
- Chokshi, A., Tielens, A. G. G. M., & Hollenbach, D. 1993, *ApJ*, **407**, 806
- Cornell, R. M., & Schwertmann, U. 2003, *The Iron Oxides: Structure, Properties, Reactions, Occurrences and Uses* (2nd ed.; Weinheim: Wiley-VCH)
- Cuzzi, J. N., Hartlep, T., Simon, J. I., & Estrada, P. R. 2017, in *Accretion: Building New Worlds, 2043* (Washington, DC: USRA), 2039
- Dominik, C., & Nübold, H. 2002, *Icar*, **157**, 173
- Dominik, C., & Tielens, A. G. G. M. 1997, *ApJ*, **480**, 647
- Draine, B. T. 1990, in *ASP Conf. Proc., The Evolution of the Interstellar Medium*, ed. L. Blitz (San Francisco, CA: ASP), 193
- Draine, B. T. 2003, *ARA&A*, **41**, 241
- Draine, B. T. 2011, *Physics of the Interstellar and Intergalactic Medium* (Princeton, NJ: Princeton Univ. Press)
- Draine, B. T., & Hensley, B. S. 2013, *ApJ*, **765**, 159
- Draine, B. T., & Hensley, B. S. 2021, *ApJ*, **919**, 65
- Dwek, E. 2016, *ApJ*, **825**, 136
- Ehrenfreund, P., Charnley, S. B., & Wooden, D. H. 2004, in *Comets II*, ed. M. C. Festou, H. U. Keller, & H. A. Weaver (Tucson, AZ: Univ. of Arizona Press), 115
- Hoang, T. 2021, arXiv:2109.07669
- Hoang, T., & Lazarian, A. 2016, *ApJ*, **831**, 159
- Hu, Z. W., & Winarski, R. P. 2016, *M&PS*, **51**, 1632
- Ishii, H. A., Bradley, J. P., Dai, Z. R., et al. 2008, *Sci*, **319**, 447
- Jones, A. P. 2001, *RSPTA*, **359**, 1961
- Jones, R. V., & Spitzer, L. 1967, *ApJ*, **147**, 943
- Keller, L. P., & Messenger, S. 2011, *GeCoA*, **75**, 5336
- Kempf, S., Pfalzner, S., & Henning, T. K. 1999, *Icar*, **141**, 388
- Kim, S-H, & Martin, P. G. 1995, *ApJ*, **444**, 293
- Li, Q., Kartikowati, C. W., Horie, S., et al. 2017, *NatSR*, **7**, 9894
- Lindquist, A. K., Feinberg, J. M., Harrison, R. J., Loudon, J. C., & Newell, A. J. 2019, *EP&S*, **71**, 5
- Martin, P. G. 1995, *ApJ*, **445**, L63
- Messenger, S., Keller, L. P., & Lauretta, D. S. 2005, *Sci*, **309**, 737
- Nesvorný, D., Jenniskens, P., Levison, H. F., et al. 2010, *ApJ*, **713**, 816
- Nesvorný, D., Li, R., Youdin, A. N., Simon, J. B., & Grundy, W. M. 2019, *NatAs*, **3**, 808
- Nuth, J. A., III, & Wilkinson, G. M. 1995, *Icar*, **117**, 431
- Özdemir, Ö., & Dunlop, D. J. 1999, *EPSL*, **165**, 229
- Planck Collaboration XI 2020, *A&A*, **641**, A11
- Poppe, A. R. 2016, *Icar*, **264**, 369
- Reisenfeld, D. B., Bzowski, M., Funsten, H. O., et al. 2021, *ApJS*, **254**, 40
- Rich, E. A., Teague, R., Monnier, J. D., Davies, C., & Bosman, H. T. J. 2021, *BAAS*, **53**, AAS237
- Roberge, W. G., & Lazarian, A. 1999, *MNRAS*, **305**, 615
- Savage, B. D., & Sembach, K. R. 1996, *ARA&A*, **34**, 279
- Sirono, S., & Ueno, H. 2017, *ApJ*, **841**, 36
- Slavin, J. D., Frisch, P. C., Müller, H. R., et al. 2012, *ApJ*, **760**, 46
- Sofia, U. J., Cardelli, J. A., & Savage, B. D. 1994, *ApJ*, **430**, 650
- Spitzer, L., Jr., & Tukey, J. W. 1951, *ApJ*, **114**, 187
- Stern, S. A., Weaver, H. A., Spencer, J. R., et al. 2019, *Sci*, **364**, eaaw9771
- Testi, L., Birmstiel, T., Ricci, L., et al. 2014, in *Protostars and Planets VI*, ed. H. Beuther et al. (Tucson: Univ. of Arizona Press), 339
- Winarski, R. P., Holt, M. V., Rose, V., et al. 2012, *Journal of Synchrotron Radiation*, **19**, 1056
- Zhukovska, S., Henning, T., & Dobbs, C. 2018, *ApJ*, **857**, 94